NOTICE CONCERNING COPYRIGHT RESTRICTIONS

Permeability Enhancement due to Cold Water Injection: A Case Study at the Los Azufres Geothermal Field, Mexico

Sally M. Benson[*], *John Daggett*[*], *Jaime Ortiz*[†] *and Eduardo Iglesias*[‡]

[*] Earth Sciences Division, Lawrence Berkeley Laboratory
Berkeley, California, USA

[†] Comisión Federal de Electricidad, Morelia, Mexico

[‡] Instituto de Investigaciones, Cuernavaca, Mexico

ABSTRACT

Pressure transient buildup and falloff data from 3 wells at the Los Azufres geothermal field have been evaluated to determine the extent to which cold water injection increases the permeability of the near-bore reservoir formation. Simultaneous analysis of the buildup and falloff data provides estimates of the permeability-thickness of the reservoir, the skin factor of the well, and the degree of permeability enhancement in the region behind the thermal front. Estimates of permeability enhancement range from a factor of 4 to 9, for a temperature change of about 150° C. The permeability enhancement is attributed to thermally induced contraction and stress-cracking of the formation.

INTRODUCTION

Injecting cold water is a common technique for estimating the permeability, productivity, and injectivity of geothermal wells. In addition to providing a measure of these parameters, there is some evidence that this practice stimulates the well (Bodvarsson et al., 1984, Benson et al., 1987). This intriguing phenomena is particularly apparent in geothermal wells in the Los Azufres geothermal field in Mexico, where a large set of pressure transient data exhibit unusual characteristics. As shown in Figure 1, it is not uncommon to observe that after an initial period during which the pressure increases as expected, the pressure stabilizes and then begins to drop, even though injection continues at a steady rate. This unusual behavior is attributed to progressive increases in the near-bore permeability. Several physical mechanisms can explain this, including; hydraulic fracturing, pushing drilling mud and formation fines away from the well-bore and into the formation, thermal contraction and thermal stress cracking of the rock, and dissolution of fracture filling minerals. As these tests were conducted well below the hydraulic fracturing gradient, this mechanism has been eliminated as a possible cause for the permeability increase, leaving one or more of the other mechanisms to account for the observed behavior.

The pressure buildup data shown in Figure 1 were analyzed by Benson et al. (1987) in an attempt to estimate the magnitude of the permeability increase needed to create the unusual pressure buildup curves. The goal of the present investigation is two-fold. First we attempt to incorporate the pressure falloff data into the analysis procedure, thereby provide more reliable estimates of the formation parameters. Next, we investigate correlations between temperature and the permeability increase in an effort to provide insight into the physical mechanism governing the near-bore permeability increase.

BACKGROUND

It is worthwhile to spend a moment reviewing the physical processes that occur as cold water is injected into a hot geothermal reservoir. First, injection causes the pressure to increase due to the formation's resistance to flow. For horizontal flow in a liquid saturated rock, the pressure buildup is governed by Equation 1

$$\nabla\cdot\left(\frac{k\rho}{\mu}\nabla p\right) = \frac{\partial(\rho\phi)}{\partial p}\frac{\partial p}{\partial t} \qquad (1)$$

where k is the formation permeability, ρ is the fluid density, μ is the fluid viscosity, p is the fluid pressure, and ϕ is the porosity of the formation. Second, as fluid is injected into the formation, an interface (called the hydrodynamic front) between the undisturbed reservoir fluid and the injected fluid moves away from the injection well. The thermal front (defined as the surface where the temperature is midway between the temperature of the reservoir and injected fluids) lags some distance behind the hydrodynamic front due to a transfer of heat from the reservoir rock to the injected fluid. The distances to the hydrodynamic and thermal fronts and the rate at which they move away from the injection well depend on the relevant mass and energy conservation equations and the geometry of the system. In the region behind the hydrodynamic and thermal fronts, the composition, temperature, compressibility (c_f) and/or density of the fluid may be different than the in-situ fluid. In addition, if the permeability, porosity, and pore-volume compressibility (c_{pv}) are temperature, stress, or composition sensitive, they too may vary in the region behind the fronts.

The wellbore also influences the pressure changes caused by injection. In deep geothermal systems the typically large wellbores create significant wellbore storage effects, resulting in a long time period before the surface and sandface injection rates are equal. Second, the wellbore acts like a large heat exchanger, transferring heat from the formation to the injected fluid before it is injected into the open interval of the well. This results in a time-varying sandface injection temperature. At moderate injection rates it may take several hours for the sandface injection temperature to stabilize.

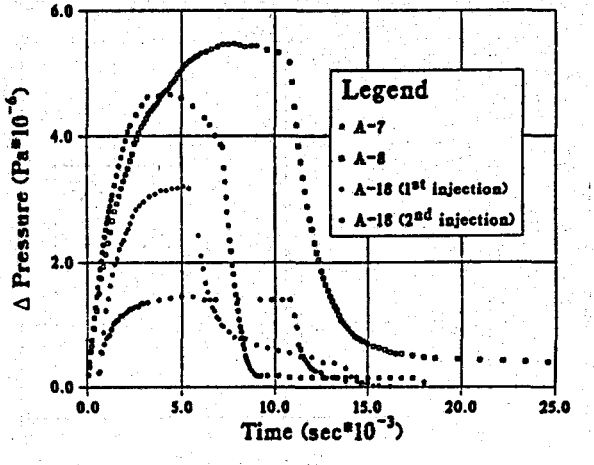

Figure 1. Pressure transient buildup and falloff data from 3 wells at the Los Azufres geothermal field, Mexico.

MATHEMATICAL MODEL

Benson et al. (1987) presented an approximate solution for calculating the pressure buildup in response to nonisothermal injection which takes the form of

$$\Delta p\,(r_w,t) = \Delta p_{ss}(r_w,t) + \Delta p_t(r_f,t) \qquad (2)$$

where $\Delta p\,(r_w,t)$ is the pressure change at the injection well, $\Delta p_{ss}(r_w,t)$ is the steady-state pressure change across the invaded region at time t, and $\Delta p_t(r_f,t)$ is the transient pressure response in the uninvaded formation. See the nomenclature at the end of the paper for a more complete description of the variables. The mathematical advantages of this form of the solution are two-fold. First, all of the non-linear terms associated with the region behind the front are incorporated into the first term of Equation 2, which for a slightly-compressible single component fluid flowing through a radially symmetric system is calculated by

$$\Delta p_{ss}(t) = \frac{q}{2\pi h}\int_{r_w}^{r_f(t)} \frac{\mu(r,t)}{k(r,t)\,\rho(r,t)}\,\frac{dr}{r} \qquad (3)$$

where q is the mass injection rate and the other terms are defined as before. Second, the term $\Delta p_t(r_f,t)$ can easily be evaluated from well established solutions such as the exponential integral solution, convolution of the instantaneous line source solution for variable flow rates, or any one of a number of solutions that satisfy the desired outer boundary conditions.

The validity of this form of the solution was discussed at length in Benson et al. (1987) and will not be reviewed here. In general, Equation 2 is valid within several seconds after injection begins, if at $t=0$, $r_f=r_w$.

ANALYSIS METHOD

Before analyzing the pressure transient data from any injection test, it is necessary to carefully assess all of the salient features of the test data. Once these have been established, a mathematical solution tailored to the problem at hand can be developed from Equations 2 and 3.

The Los Azufres geothermal system occurs in fractured volcanic rocks, at a depth of 1000 to 2000 m. Reservoir temperatures range from 220 to 280 °C in the wells from which injection test data are available. Geothermal fluids are produced from fractured units within andesitic rocks. The injection tests consisted of injecting 20 °C water into the formation at a constant wellhead injection rate for 2 to 3 hours. During injection, the formation pressure was measured with an Amerada pressure gauge positioned adjacent to the production zone in the well.

Pressure versus time graphs of the pressure buildup and falloff data shown in Figure 1 indicate that wellbore storage effects persist throughout the entire 2 to 3 hour test. This is illustrated in Figure 2, which shows the sandface injection rate as a function of time for well A-8. For the first half of the injection period, the sandface injection rate gradually increases to the surface injection rate. During the latter half of the injection, the sandface injection rate is greater than the surface injection rate because the pressure (water-level) is dropping in the wellbore.

Another factor that must be considered is that although the temperature of the injected water is constant at the wellhead, it is not constant at the formation face. As shown by the simulated sandface injection temperature in Figure 3, the actual sandface temperature will decrease throughout the test. By the end of the test, the temperature is still nearly 70 °C above the surface temperature. The time-varying injection temperature causes the fluid viscosity (see Figure 4) and density to vary throughout the test. This creates a non-uniform distribution of the fluid properties in the region behind the thermal front.

Solution Technique

To develop a mathematical solution for calculating the pressure buildup, we must first describe how the thermal front moves with time. For the purposes of this analysis, the distance to the thermal front is estimated from the energy balance for piston-like displacement of cold water into a hot water formation. From this simple approximation we obtain

$$r_f^2 = \frac{\rho_w C_w}{\rho_a C_a}\,\frac{1}{\pi h}\int_0^t Q(t)dt \qquad (4)$$

where C_w and C_a are the heat capacities of water and the formation respectively, and the other terms are as defined previously. Note that this formulation assumes that there is no heat transfer between the unfractured matrix blocks and the permeable fracture zones into which fluid is injected. Although this is not generally true for fractured reservoirs, this assumption is justified in light of the short duration of the tests and that the fluid is injected into a "fracture zone" that is much thicker than the apertures of individual fractures. If the fluid is injected into very thin strata, separated by much thicker ones, the effects of heat conduction to the surrounding strata must be considered (Bodvarsson and Tsang, 1982).

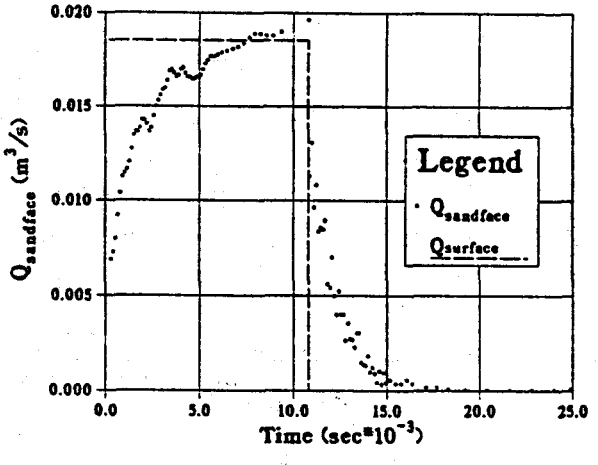

Figure 2. Sandface and surface injection rates for well A-8.

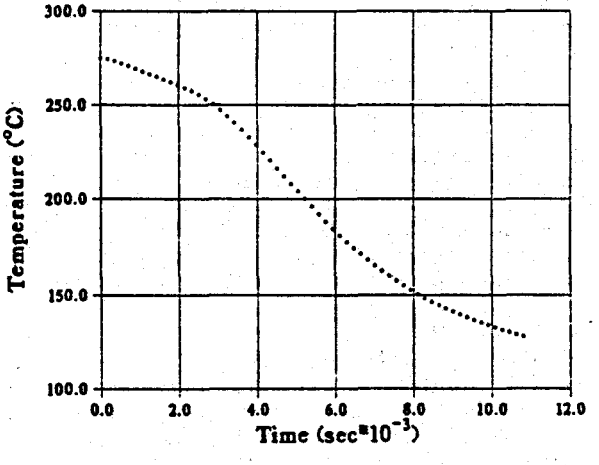

Figure 3. Sandface injection temperature in well A-8, calculated using a wellbore simulator.

It is also necessary to describe how the fluid properties vary behind the front. For this study we assume that the fluid viscosity and density, as well as the formation permeability, vary linearly in the region behind the front

$$\mu_i(r,t) = \mu_i(r_w,t) + \frac{\mu_r - \mu_i(r_w,t)}{r_f - r_w}(r - r_w) \quad (5a)$$

$$\rho_i(r,t) = \rho_i(r_w,t) + \frac{\rho_r - \rho_i(r_w,t)}{r_f - r_w}(r - r_w) \quad (5b)$$

$$k_i(r,t) = k_i(r_w,t) + \frac{k_r - k_i(r_w,t)}{r_f - r_w}(r - r_w) \quad (5c)$$

By substituting Equations 5a to 5c into Equation 3, we can calculate the steady-state pressure buildup in the region behind the front from

$$\Delta p_{ss}(t) = \frac{q(t)}{2\pi h}\left\{\frac{\mu_i(r_w,t)}{k_i(r_w,t)\rho_i(r_w,t)}\ln\frac{r_f}{r_w} + \left[\frac{\mu_r}{k_r\rho_r} - \frac{\mu_i(r_w,t)}{k_i(r_w,t)\rho_i(r_w,t)}\right]\left[1 - \frac{r_w}{r_f - r_w}\ln\frac{r_f}{r_w}\right]\right\} \quad (6)$$

To develop a complete solution to Equation 2 we also need an expression for calculating the transient pressure response in the uninvaded region of the reservoir. For this study we assume that the reservoir is approximately described as a uniform porous media, of infinite areal extent, and bounded above and below by impermeable strata. For this type of system, the second term of Equation 2 can be evaluated if the time-varying flow rate is represented by a sequence of straight line segments, each of the proper duration and slope (McEdwards and Benson, 1981). The full solution to Equation 2 is calculated by adding Equation 6 to the pressure transient response in the outer region. A computer program, INJECT, that performs the necessary calculations has been written (Daggett and Benson, 1988).

Analysis Procedure

Three primary variables must be determined to analyze the pressure buildup tests. These include the permeability-thickness-viscosity term ($k_r h/\mu_r$) of the fracture zones, the porosity-compressibility-thickness-skin factor term ($\phi c h e^{-2s_m}$, where s_m is the mechanical skin factor of the well), and the magnitude of the near-bore permeability enhancement. A three-stage analysis method is required for evaluating all of these parameters.

First $k_r h/\mu_r$ is calculated from a history-match of the late-time pressure falloff data. The late time interval is used because during this period the downhole pressure response is almost entirely governed by the region outside the thermal front. Figure 2 shows that this period begins around 1.8×10^4 s into the test.

Second, the estimate of $k_r h/\mu_r$ is refined and the mechanical skin factor of the well is determined by history-matching the early time pressure buildup data when the nonisothermal effects are small. As shown by Figures 3 and 4, the early (isothermal) part of the pressure buildup lasts approximately 900 s.

Finally, after establishing $k_r h/\mu_r$ and s_m, the remainder of the test data are used to calculate the magnitude of the near-bore permeability changes that occur as the progressively colder water is injected into the formation. The procedure for doing this is as follows. First, the pressure buildup ($\Delta p_i(r_w,t)$) for an isothermal injection test (at the formation temperature) is calculated using the formation parameters obtained from the initial steps in the analysis procedure. Next, the difference between $\Delta p_i(r_w,t)$ and the actual pressure response is used to calculate the near-bore permeability change from the following expression

$$\frac{k_r}{k_i(r_w,t)} = \frac{\mu_r \rho_i(r_w,t)}{\mu_i(r_w,t)\rho_r} \times \left\{\frac{\frac{2\pi k_r \rho_r h}{q\mu_r}\left[\Delta p(r_w,t) - \Delta p_i(r_w,t)\right] - s_{ma} + s_m}{\left[\left(1 + \frac{r_w}{r_f - r_w}\right)\ln\frac{r_f}{r_w} - 1\right]} + 1\right\} \quad (7)$$

where s_{ma} is the apparent-mechanical skin factor of the well. For $s_m > 0$

$$s_{ma} = \frac{\mu_i(r_w,t)\rho_r}{\mu_r\rho_i(r_w,t)} s_m \quad (8a)$$

and for $s_m \ll 0$

$$s_{ma} = s_m \quad (8b)$$

(Benson, 1984).

Each of the four injection tests shown in Figure 1 have been analyzed using the above procedure.

Well A-8 Analysis

The injection test data for well A-8 are shown in Figure 5. The sandface injection rate, temperature, and fluid viscosity are shown in

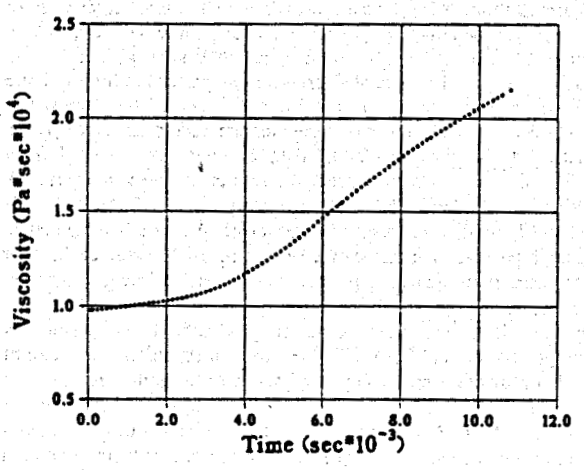

Figure 4. Sandface viscosity of the injected fluid in well A-8.

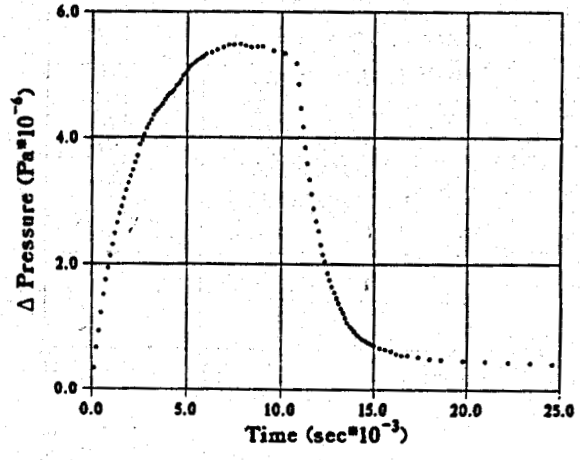

Figure 5. Pressure buildup and falloff data for well A-8.

Figures 2 through 4, respectively. For the first 15 minutes of the test, the bottomhole temperature remained at approximately 275 °C. A history-match of the falloff data and the first 900 s of the buildup data yields a $k_r h$ of 4.9×10^{-13} m^3 and a mechanical skin factor of +1. After the first fifteen minutes, the temperature sensitive rock and fluid properties begin to influence the data. Using the procedure outlined above, the ratio of the undisturbed formation permeability to that of the invaded region immediately adjacent to the wellbore is calculated for the rest of the test period. The results of these calculations are shown in Figure 6, where the ratio of $k_i(r_w,t)/k_r$ is plotted as a function of time from the beginning of the injection test. The ratio is plotted for a range of values for the formation thickness because we do not have an accurate measure of the thickness of the zone(s) into which the fluid is injected. The figure shows that during the test the permeability of the near-bore region must increase by a factor ranging from about 4 to 8, depending on the actual thickness of the formation. Figure 6 also demonstrates that if the formation thickness is less than 50 m, the results of the calculation are relatively insensitive to the actual value of the formation thickness. The fractured nature of the producing formation and the occurrence of discrete loss-of-circulation zones encountered while drilling suggest that the actual thickness is in the range of 5 to 10 m. Thus, the permeability appears to increase by a factor of 4 over the test period.

Once the formation parameters and the magnitude of the near-bore permeability increases are determined, these calculations can be double-checked by comparing the measured pressure response to the calculated response (see Fig. 7).

Another source of uncertainty in this analysis is the actual distribution of the fluid and rock properties within the invaded region. As indicated by Equations 5a-c, we assume that these vary linearly. To test the restraints imposed on the analysis by this assumption, we repeated these calculations for the case where the fluid and rock properties are constant throughout the invaded region. The results of these calculations are shown in Figure 8. These calculations show that the results are relatively insensitive to the presumed distribution of the various parameters. This is explained in light of the dominating influence of the very near-well region on the pressure response, which is nearly the same, regardless of how the properties vary farther away from the well.

Well A-7 Analysis

The injection test data for well A-7 are shown in Figure 1. The sandface injection rate, temperature, and fluid viscosity are shown in

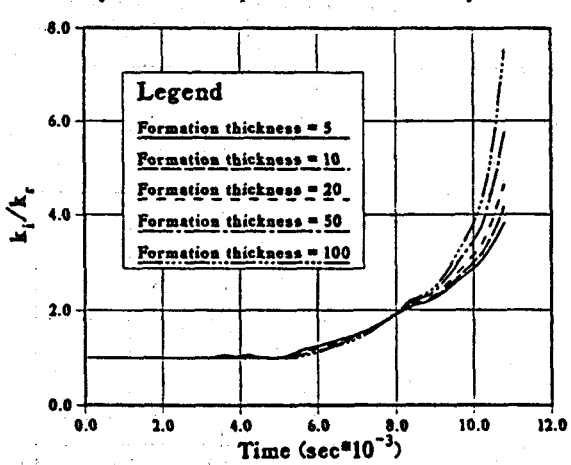

Figure 6. Calculated near-bore permeability enhancement during the nonisothermal injection test in well A-8. Calculated values are presented for the range of thicknesses (in meters) listed.

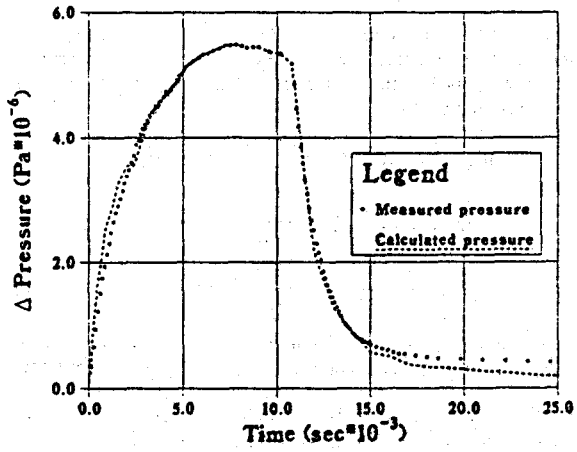

Figure 7. Match between the measured and calculated pressure transient response in well A-8.

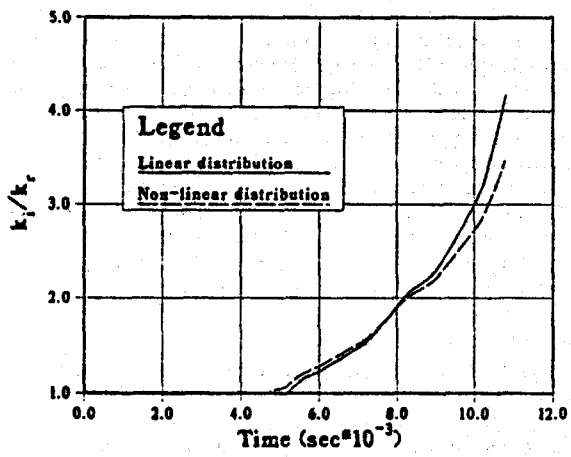

Figure 8. Comparison between the calculated permeability enhancement for a "sharp" front (Non-linear) and a diffuse thermal front (Linear) in well A-8.

Figures 9 through 11. This test illustrates that in some cases it is not possible to obtain a good match for the entire test and that a compromise must be reached in matching the early, middle, and late-time data. The calculated pressure buildup and falloff in Figure 12 was calculated using a $k_r h$ of 3.0×10^{-13} m^3. The figure shows that a good match of the early time pressure data is achieved, yet the match of the pressure falloff data is poor. A higher $k_r h$ of 7.5×10^{-13} m^3 was then used; the results are seen in Figure 13. Using this higher $k_r h$, a better history-match of the falloff is achieved, but this also results in a poor early pressure buildup match. A large positive skin factor of 2.5 could be used to correct the poor early pressure match, but this causes the difference between $\Delta p_i(r_w,t)$ and the actual pressure response to become so large that the calculated near-bore permeability change is unrealistic. A compromise ($k_r h$ of 6.9×10^{-13} m^3 and a mechanical skin factor of 0) that provides a reasonably good match of the entire test is shown in Figure 14. The calculated near-well permeability enhancement for each of the above cases is plotted as a function of the temperature change in Figure 15. The figure suggests that there must be a near-bore permeability increase affecting the downhole pressure response regardless of the exact values of the assumed parameters.

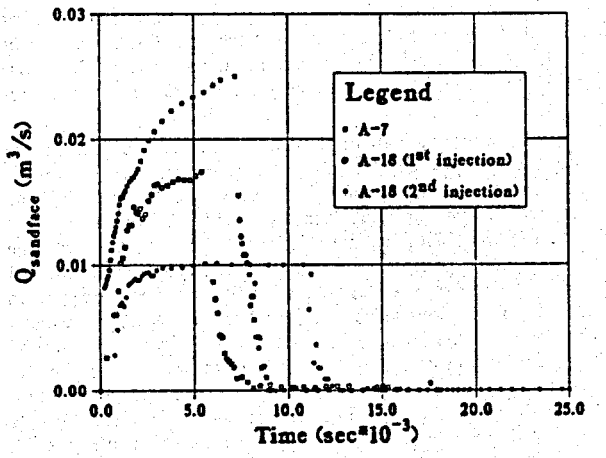

Figure 9. Pressure buildup and falloff for wells A-7 and A-18 (two tests).

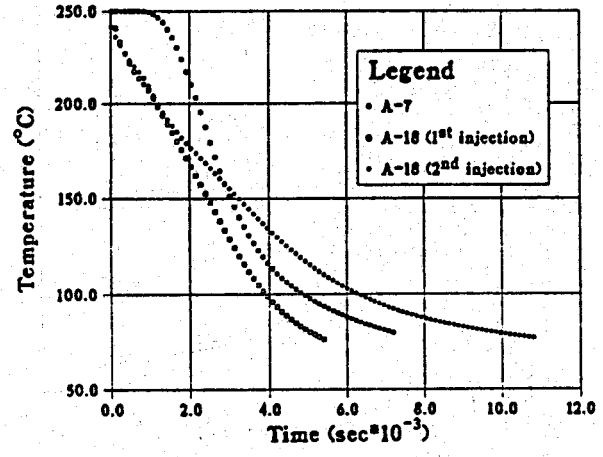

Figure 10. Sandface injection temperatures for well A-7 and A-18 (two tests).

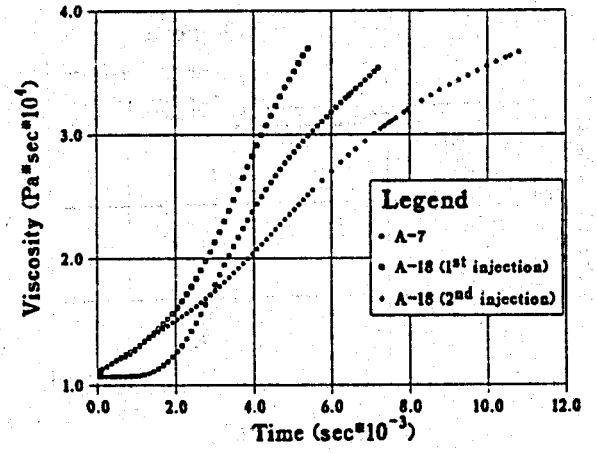

Figure 11. Sandface viscosities for wells A-7 and A-18 (two tests).

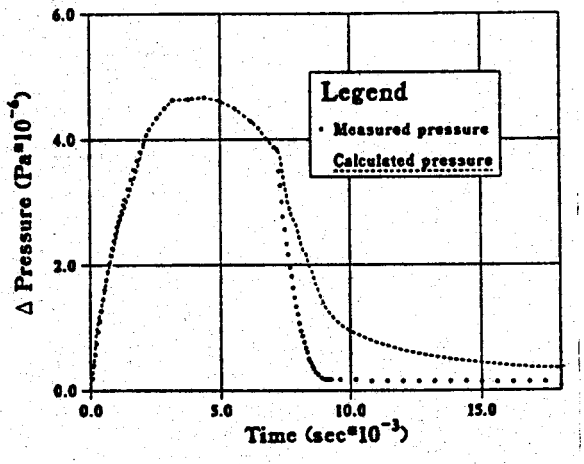

Figure 12. One possible match of the A-7 injection test data. Note the good match of the buildup data and the poor match of the falloff data. Parameters for this match are $k_r h/\mu_r = 2.8\times10^{-9}$ $m^3/Pa\cdot s$, $\phi c_t h = 2\times10^{-8}$ m/Pa, and s=−2.

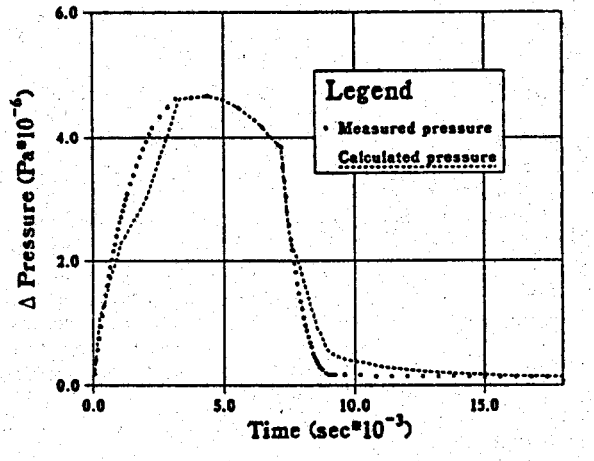

Figure 13. One possible match of the A-7 injection test data. Note the poor match of the buildup data and the better match of the falloff data. Parameters for this match are $k_r h/\mu_r = 7.0\times10^{-9}$ $m^3/Pa\cdot s$, $\phi c_t h = 2\times10^{-9}$ m/Pa, and s=0.

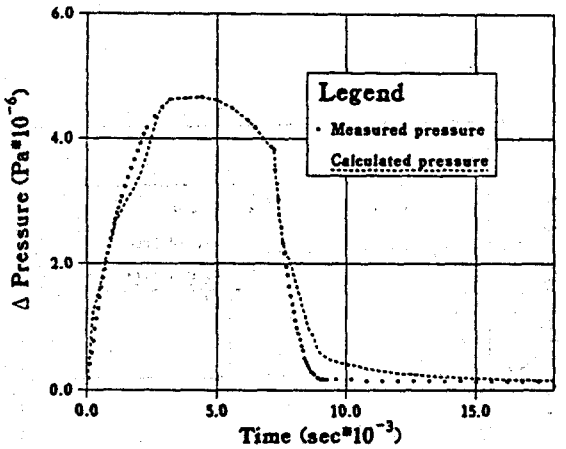

Figure 14. Best match of the A-7 injection test data. Parameters for this match are $k_r h/\mu_r = 6.5\times10^{-9}$ m^3/Pa·s, $\phi c_t h = 7\times10^{-10}$ m/Pa, and s=0.

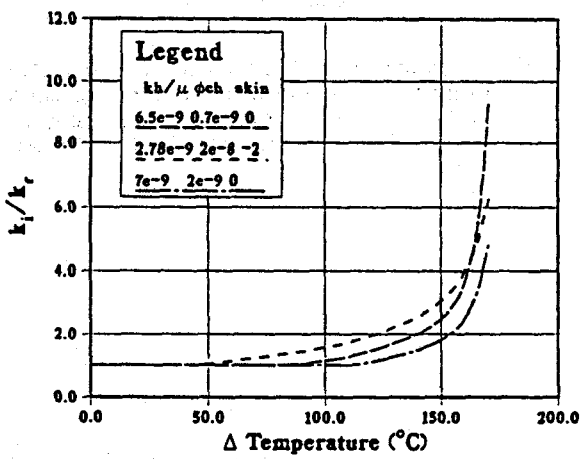

Figure 15. Calculated permeability enhancement for well A-7 for the three history-matches shown in Figures 12, 13, and 14.

An alternative explanation of the well A-7 data is also possible. Perhaps, as indicated by the relatively high formation permeability required to fit the pressure falloff data, one or more fracture zones began accepting fluid during the middle of the test, thereby, increasing the overall $k_r h$ of the well, as opposed to simply increasing the permeability of already open fractures. Without additional information, such as a succession spinner surveys, it is not possible to resolve which explanation is the correct one.

Well A-18 Analysis

Several consecutive injection tests were conducted in well A-18, two of which are analyzed here (see Fig. 9). These two tests took place only three days apart, on May 30 and June 2, 1980. The sandface injection fluid temperatures for both tests were therefore calculated as one continuous 72 hour test. This was done in order to take into account any cooling during the first test which may have resulted in a lower bottomhole temperature at the beginning of the second test. The bottomhole temperatures at the start of the first and second injection tests are 250 and 242 °C, respectively. Sandface fluid flowrates, temperatures, and viscosities are shown in Figures 9 through 11 for both of these tests.

History-matches of test data yield a $k_r h$ and skin of 2.6×10^{-13} m^3 and -1.7 for the first test and a $k_r h$ and skin of 9.6×10^{-13} m^3 and 1.2 for the second test, respectively. Comparisons of the calculated and measured pressure data are shown in Figures 16 and 17.

Unfortunately, both of these injection tests are difficult to analyze. The pressure falloff from the first test has a two-part recovery, where mid-way through the recovery phase the falloff rate increased significantly. Data from the second falloff test are unusual because the final recovery pressure was 2×10^5 Pa lower than the initial pressure. Perhaps formation heterogeneity and/or internal flow in the wellbore is responsible for the observed behavior. In addition to the above-mentioned complexities, we can not explain why the $k_r h$ of the formation is nearly 3 times higher for the second test than it is for the first test. The test records indicate that the precise depth of the well was not known at the time of the second test. Perhaps a greater open interval with additional fractured intervals was tested. In spite of these difficulties, as illustrated in Figure 18, data from both tests indicate significant near-bore permeability enhancement occurred during the injection tests.

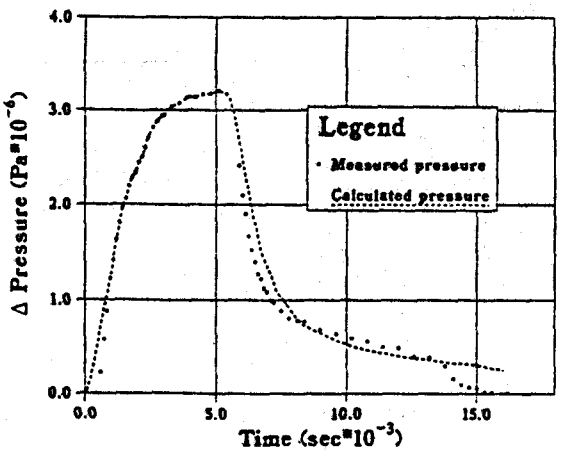

Figure 16. History-match of the first injection test in well A-18.

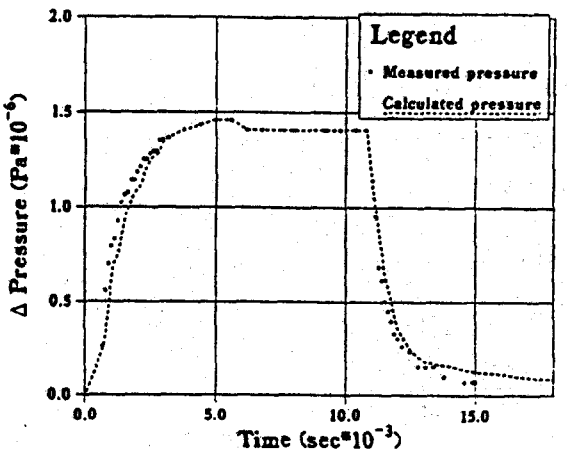

Figure 17. History-match of the second injection test in well A-18.

RESULTS

The magnitude of the near-bore permeability enhancement in each of the 3 test wells (A-7, A-8, and A-18) is plotted as a function of sandface injection temperature decrease in Figure 18. The calculated permeability increases for all the wells are remarkably similar, suggesting that the correlation between the sandface injection temperature and the permeability increase is attributable to lowering the temperature of the near-bore reservoir formation.

There are several possible explanations for the observed temperature versus permeability relationship, including thermal stress cracking, dissolution of the formation, and thermal contraction of the rock matrix. In the absence of additional information, we cannot determine which of these possibilities is the correct one, or if a single mechanism is responsible for the observed pressure behavior. Recent laboratory studies of thermal stress cracking indicate that both intragranular and grain-boundary stress cracks can develop in the downhole thermal regime created by these injection tests (Fredrich and Wong, 1986). Analysis of field experiments at the hot-dry-rock site at Fenton Hill, New Mexico, indicate that "reservoir growth" can be at least partially attributed to thermally induced stress cracks (Tester et al., 1986). It is likely that a similar mechanism is responsible for the permeability enhancement reflected by the data described here.

The analysis presented here is just the beginning of a series of studies that must be conducted if we are to improve our understanding of the physical phenomena that accompany waste brine reinjection into geothermal reservoirs. To date, we do not have an adequate understanding of the physical mechanisms causing the unusual pressure transient responses nor the observations that well injectivity is often better than anticipated. The possibility that the observed permeability increases may be permanent or semi-permanent is also intriguing. If so, cold water injection may come to be considered as a bona fide stimulation treatment for geothermal wells.

CONCLUSION

Analysis of injection test data from three wells at the Los Azufres geothermal field in Mexico indicate that the permeability of the near-bore region increases during cold water injection. Careful examination of the data reveal that an accurate analysis of the data is impossible if wellbore storage effects and thermal transients in the wellbore are not accounted for. By using a new analysis method outlined here, the magnitude of the permeability increase that is required to match the observed pressure transient data is calculated. These analyses indicate that the permeability increases in the near-bore region by approximately a factor of 4 to 9 during the 2 to 3 hour period when cold water is injected into the formation. Concurrent analysis of the buildup and falloff data provides for a greater degree of confidence in these results than was provided from analysis of the buildup data alone. A good correlation between the permeability increase and the sandface injection temperature indicates that the permeability increase is caused by cooling the near-bore reservoir formation. Thermal contraction and thermal stress cracking of the formation are the most probable cause of the near-bore permeability increase.

ACKNOWLEDGEMENTS

The authors gratefully acknowledge Marcelo Lippmann for reviewing this paper. This work is supported through the U.S. Department of Energy Contract No. DE-AC03-76SF00098 by the Assistant Secretary for Conservation and Renewable Energy, Office of Renewable Technology, Division of Geothermal Technology.

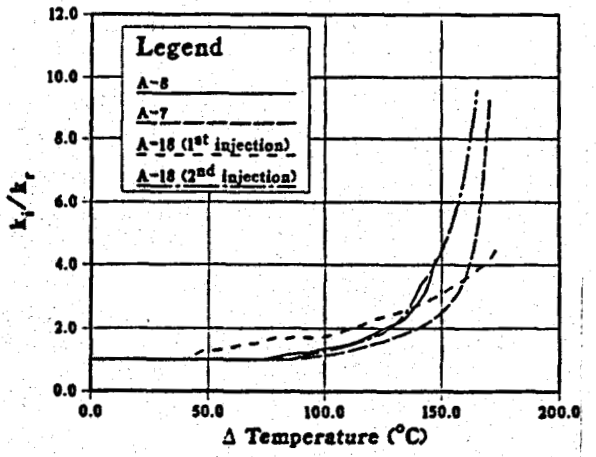

Figure 18. Calculated values for the permeability increase in the near-wellbore region for three wells at the Los Azufres Geothermal Field, Mexico.

NOMENCLATURE

c_f	fluid compressibility (1/Pa)
c_{pv}	pore-volume compressibility (1/Pa)
C_a	heat capacity of the aquifer (J/kg/° C)
C_w	heat capacity of the injected water (J/kg/° C)
h	thickness of the injection zone (m)
k	permeability (m^2)
$k_i(r_w,t)$	sandface formation permeability (m^2)
k_r	permeability of the injection zone(s) (m^2)
p	pressure (Pa)
$\Delta p(r_w,t)$	pressure change at the wellbore (Pa)
$\Delta p_{ss}(r_w,t)$	pseudo-steady-state pressure change across the invaded region (Pa)
$\Delta p_i(r_f,t)$	transient pressure change at r_f in the uninvaded formation (Pa)
r	distance from the wellbore (m)
r_f	distance to the thermal front (m)
r_w	wellbore radius (m)
t	time (s)
ϕ	porosity (-)
μ	fluid vicosity (Pa·s)
$\mu_i(r_w,t)$	fluid vicosity at the sandface (Pa·s)
μ_r	vicosity of the reservoir fluid (Pa·s)
ρ	fluid density (kg/m^3)
$\rho_i(r_w,t)$	fluid density at the sandface (kg/m^3)
ρ_r	density of the reservoir fluid (kg/m^3)

REFERENCES

Benson, S.M., 1984. Analysis of Injection Tests in Liquid-Dominated Geothermal Reservoirs. M.S. Thesis, University of California, Berkeley. Lawrence Berkeley Laboratory Report, LBL-17953, Berkeley, California.

Benson, S.M., J.S. Daggett, E. Iglesias, V. Arellano, and J. Ortiz, 1987. Analysis of Thermally Induced Permeability Enhancement in Geothermal Injection Wells. Proceedings, 12th Workshop, Geothermal Reservoir Engineering, Stanford, California.

Daggett, J. S., and S. M. Benson, 1988. User's Guide For Inject, A Computer Code For Calculating Pressure Transients During Nonisothermal Injection Tests. Lawrence Berkeley Laboratory Report, LBL-24718.

Bodvarsson, G.S., Benson, S.M., Sigurdsson, O., Stefansson, V., and Eliasson, E.T., 1984. The Krafla Geothermal Field, Iceland: 1. Analysis of Well Test Data, *Water Resources Research*, Vol 20, No. 11, pp. 1515-1530.

Bodvarsson, G.S. and Tsang, C.F., 1982. Injection and Thermal Breakthrough in Fractured Geothermal Reservoirs, *Journal of Geophysical Research*, Vol. 84, No. B2, pp. 1031-1048.

Fredrich, J.T., and Wong, T., 1986. Micromechanics of Thermally Induced Cracking in Three Crustal Rock, *Journal of Geophysical Research*, Vol. 91, No. B12, pp. 12743-12764.

McEdwards, D.G. and Benson, S.M., 1981. User's Manual for ANALYZE-- A Variable-Rate, Multiple Well, Least Squares Matching Routine for Well Test Analysis, Lawrence Berkeley Laboratory Report, LBL-10907, Berkeley, California.

Ramey, H.J. Jr., 1970. Approximate Solutions for Unsteady Liquid Flow in a Composite Reservoir, *Journal of Canadian Petroleum Technology*, March, 1970, pp. 32-37.

Tester, J.M., Murphy, H.D., Potter, R.M., and Robinson, B.A., 1986. Fractured Geothermal Reservoir Growth Induced By Heat Extraction. Society of Petroleum Engineers Paper SPE-15124. Presented at the 56th California Regional Meeting of the Society of Petroleum Engineers, Oakland, California, April 2-4, 1986.